Chemosphere 251 (2020) 126369

Contents lists available at ScienceDirect

Chemosphere

journal homepage: www.elsevier.com/locate/chemosphere

Multi-edged molybdenite achieved by thermal modification for enhancing Pb(II) adsorption in aqueous solutions

Yuan Yuan [a], Weiquan Zhan [a], Feifei Jia [a, *], Shaoxian Song [a, b]

[a] Hubei Key Laboratory of Mineral Resources Processing and Environment, Wuhan University of Technology, Luoshi Road 122, Wuhan, Hubei, 430070, China
[b] School of Resources and Environmental Engineering, Wuhan University of Technology, Luoshi Road 122, Wuhan, Hubei, 430070, China

HIGHLIGHTS

- M-400 achieved 147.8 mg/g Pb (II) adsorption in aqueous solutions.
- Thermal modification enabled molybdenite with a 10 times enhancement on Pb (II) adsorption compared with natural molybdenite.
- Sulfur vacancies on edges had strong affinity to Pb ions.

GRAPHICAL ABSTRACT

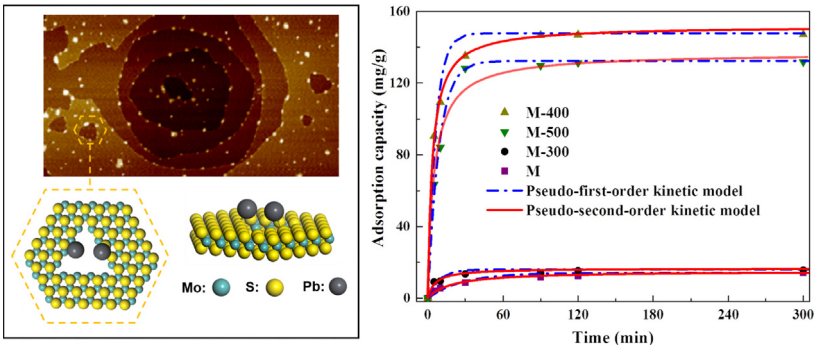

ARTICLE INFO

Article history:
Received 1 January 2020
Received in revised form
22 February 2020
Accepted 26 February 2020
Available online 29 February 2020

Handling Editor: Grzegorz Lisak

Keywords:
Multi-edged molybdenite
Pb(II) adsorption
Thermal modification
Sulfur vacancy

ABSTRACT

Thermal modification was simply performed on molybdenite to enhance the adsorption of Pb(II) in aqueous solutions, and the root of this phenomenon was well studied in this work. Various thermal modification temperatures at 300 °C, 400 °C and 500 °C were applied to modify the surface property of molybdenite, producing different degrees of edge defect and surface wettability in molybdenite samples. Contact angle tests, atomic force microscopy (AFM) observations and adsorption tests illustrated that molybdenite thermally modified at 400 °C contained most edge defects and achieved a 147.846 mg/g Pb(II) adsorption, which was almost 10 times of that obtained by natural molybdenite. The adsorption experiment also indicated that the increase of surface hydrophilia of molybdenite would slightly benefit the Pb(II) adsorption. The X-ray photoelectron spectroscope (XPS) exhibited that a strong chemical adsorption existed between Pb(II) and S elements. AFM study further demonstrated that the interaction between Pb(II) and S atoms exposed at the triangular edges of molybdenite were the intrinsic reason for the great enhancement of Pb(II) adsorption. This work provides a new insight to absorb Pb(II) in aqueous solutions using natural molybdenite.

1. Introduction

For decades, a growing attention has been paid on the management as well as control of environmental pollution (Huang et al., 2017; Manohar et al., 2002; Zhang et al., 2019). As one of the

* Corresponding author.
E-mail address: feifeijia@whut.edu.cn (F. Jia).

https://doi.org/10.1016/j.chemosphere.2020.126369
0045-6535/

hazardous materials on earth, heavy metals like cadmium, mercury and lead (Huang et al., 2020; Lisak et al., 2012) can be found in water, soil, plants and even in animal bodies, which has been a huge threat to environment through the ages (Feng et al., 2017; Sdiri et al., 2012; Zeng et al., 2019). For example, lead is well known as a harmful element which can induce a series chronic and lethal disorders to human nervous system, brain tissue and the reproductive system (Abbaspour et al., 2010; Hu et al., 2016; Mondal et al., 2018). Thus, the methods to remove those heavy metal from wastewater has been a challenge which attract great attention around the world (Gatabi et al., 2020; Wang et al., 2017; Yin et al., 2016). Among the existing technologies including precipitation (Alvarez et al., 2007), ion-exchange (Jeffrey et al., 2010) and electrodes (Ding et al., 2019; Lisak et al., 2012; Saénz et al., 2010) of removing Pb(II), absorption of heavy metals from solution, as one of the conventional techniques for solving this problem, has been wildly used due to its simplicity, high efficiency and low cost - as long as targeted absorbents can be advisably applied (Jia et al., 2017; Peng et al., 2016; Xu et al., 2017; Zhu et al., 2018). Hence, the procedure to find solutions can be simply reduced to searching for proper absorbent aiming at different heavy metals.

In view of the Pearson Hard Soft Acid Base (HSAB) principle, lead, was a soft acid, which could interact with soft bases such as reduced-S ligands. Although sulfur resources have been introduced into various materials for enhancing the adsorption of Pb(II) ions in aqueous solutions, it was hard to apply these materials in practical applications due to the complex preparation step and expensive synthesized raw materials. Therefore, it was urgent to find a kind of cheap material contains rich sulfur atoms for removing Pb(II) ions from aqueous solutions.

Molybdenum disulfide, with a chemical composition of MoS_2, has been wildly used as a typical Layered Transition Metal Disulfides (TMDs) owing to its good lubricity, catalysis and photoelectric performance (Ai et al., 2016). Natural molybdenite is mainly composed of MoS_2 with relatively low price because it was one kind of the earth-abundant mineral materials. Molybdenite has a special layered structure with the sandwiched atomic arrangements (S-Mo-S) in which the weak van der Waals forces combine with each other, which endows MoS_2 with plenty of S atoms when torn apart to expose flatten facets (Hong et al., 2014; Sun et al., 2019; Tang et al., 2018). Due to the high affinity and selectivity of MoS_2 for soft-acid heavy metal ions (Hong et al., 2019; Kumar et al., 2019; Liu et al., 2019; Wang et al., 2018), molybdenite is a prospective adsorbent for removing Pb(II) ions in aqueous solutions. However, the pristine molybdenite contains relatively less S vacancies which are reported to be the active cites during the absorption proceeding (Gao et al., 2015). Hence, it's of great importance to explore methods to allow MoS_2 with plenty of S vacancies, *i.e.*, active absorption cites to improve the heavy metal ions adsorption capacity of MoS_2.

Here, in our work, thermal modification was applied to produce large quantities of S vacancies on edges of molybdenum disulfide. Here, in our work, thermal modification was applied to produce large quantities of S vacancies on edges of molybdenum disulfide. Different temperatures (300, 400 and 500 °C) were performed on molybdenite for its thermal modification, and the detailed variations on structure, morphology, chemical element states and surface hydrophobicity of molybdenite under different thermal modification conditions were firstly investigated. The mechanism of S vacancies on MoS_2, as well as the affect factors in Pb(II) absorption was well explored. The X-ray diffraction (XRD) and Raman tests were used to analyze the influence of thermal modification on the structure of MoS_2. What's more, the atomic force microscopy (AFM), scanning electron microscopy (SEM) and energy-dispersive spectra (EDS) were applied to observe the morphology differences. Absorption kinetics experiments were used to compare the different absorption capacity of Pb(II). At last, X-ray photoelectron spectroscopy (XPS), AFM, SEM and EDS were obtained to analyze the absorption adsorption mechanism.

2. Experimental

2.1. Materials

Natural molybdenite used in this work was obtained from Wuzhou Mine (Guangxi Province, China). Lead nitrate ($Pb(NO_3)_2$), sodium hydroxide (NaOH) and nitric acid (HNO_3) of analytical purity with 99% were brought from Sinopharm Chemical Reagent Co., Ltd (Shanghai, China). Milli-Q water (Millipore SAS, France) was used in the whole experiment with 18.2 MΩ cm.

2.2. Thermal modification of molybdenite

Molybdenite was modified by a simple thermal treatment route (Jia et al., 2018a). Firstly, 10 g of molybdenite with particle size of 45 μm was put in a ceramic crucible. Then, the crucible was placed into a muffle furnace (Vulcan 3-550) where the sample was heated from normal temperature to a certain value (300, 400 and 500 °C) with the heating rate of 10 °C/min. After being cooled down to the normal temperature, the samples were washed with distilled water and filtrated. All the products were named as M-X, where X exhibited the thermal treatment temperature of molybdenite.

2.3. Pb(II) adsorption experimental

Batch experiments of Pb(II) on molybdenite with and without thermal treatment were performed in conical flasks at normal temperature. Adsorption kinetics studies of Pb(II) on adsorbents were performed at pH of 5.00 ± 0.5 (adjusted by NaOH or HNO_3) with Pb(II) concentration of 100 mg/L. In the adsorption experiment, 250 mg of adsorbents were added into Pb(II) solution and then the mixture was with mechanical shaken at 150 rpm. After that, at predetermined time intervals, 5 mL suspension was extracted out and filtered using filter membrane (0.22 μm), first 2 mL was discarded to minimize the effect of impurity and the left 3 mL was diluted to appropriate concentrate for AAS analysis. Adsorption capacity of Pb(II) was calculated on the basis of the following equation:

$$q = \frac{C_0 V_0 - CV}{m} \quad (1)$$

where q was adsorption capacity, mg/g; V_0 and V represented the volume of Pb(II) solution before and after adsorption, respectively, L; C_0 and C exhibited the Pb(II) concentration before and after adsorption, respectively, mg/L; m was the amount of adsorbent, g.

2.4. Characterization

XRD patterns of samples were obtained on a D8 Advance X-ray diffractometer. Zeiss Gemini 300 was used to obtain SEM images corresponding EDS of samples. XPS was acquired on ESCALB 250Xi photoelectron spectrometer. A Netzsch Sta 449F3 simultaneous thermal analyzer was applied for analyzing the thermostability of molybdenite in air atmosphere with the heating rate of 10 °C/min from normal temperature to 1000 °C. The surface morphologies of samples were observed by a Bruker MultiMode 8 AFM (USA) with Peak Force Tapping mode. The concentration of Pb(II) was detected using a Perkin-Elmer Analyst 700 atomic absorption

spectrophotometer. Raman patterns were recorded by INVIA Raman microscope. To measure the adsorbents after adsorption, the samples were carefully washed with deionized water for several times to remove the un-adsorbed ions on the surface.

3. Results and discussion

3.1. Characterization of molybdenite after thermal modification

XRD patterns of molybdenite before and after thermal modification were exhibited in Fig. 1. The diffraction peaks of all the samples corresponded well with the (002), (100), (103), (105) and (110) reflections at 2θ = 14.4°, 32.7°, 39.6°, 49.8° and 60.1° (JCPDS No. 37-1492), which demonstrated the formation of hexagonal MoS_2 phase (Zhan et al., 2020). No impurity signals were detected, indicating the high purity of the samples. In addition, the corresponding *d* spacing of M, M-300, M-400 and M-500 were all around 6.2 Å. The results showed XRD patterns before and after thermal modification, which did not show significant differences, indicating that thermally modification would not affect the crystal structure of molybdenite.

Fig. 2 exhibited the Raman spectrum of molybdenite before and after thermal treatment. The characteristic in-plane E_{2g} mode and out-of-plane A_{1g} mode of molybdenite appeared in all samples. After thermal treatment of molybdenite, slight Raman shifts occurred on the peaks, demonstrating the thickness of molybdenite changed (Jia et al., 2018a, 2018b).

The morphologies and microstructures of M, M-300, M-400 and M-500 were examined in detail with the aid of SEM, TEM and AFM. As exhibited in Fig. 3, all the samples displayed the flake structure. Compared with the morphology of pristine molybdenite, it was obvious that the surfaces of molybdenite after thermal treatment became smoother as the thermal treatment temperature increased, which might originate from the exposure of fresh surface. Fig. 4 showed transmission electron microscopy (TEM) and high-resolution transmission electron microscopy (HRTEM) images of molybdenite without thermal treatment and thermally treated at 400 °C. It could be seen that molybdenite without thermal treatment and thermally treated at 400 °C possessed almost same flake morphology and interlayer spacing. However, it was hard to research the surfaces at atomic scale through SEM and TEM, thus AFM was applied for further investigating the microcosmic surface

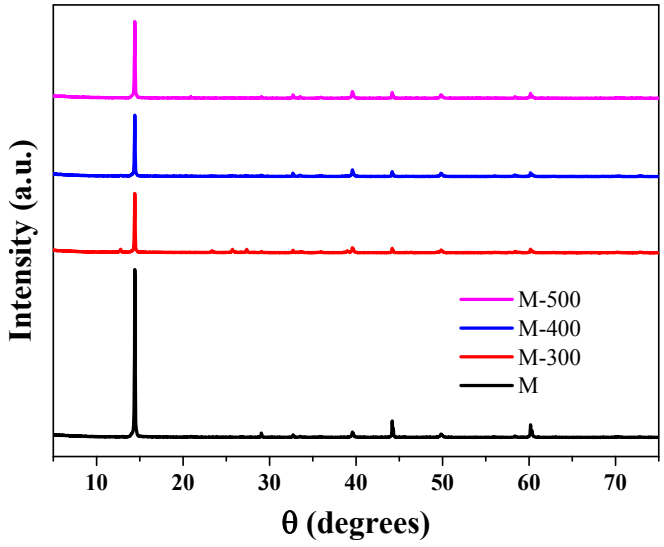

Fig. 1. XRD patterns of molybdenite before and after thermal treatment.

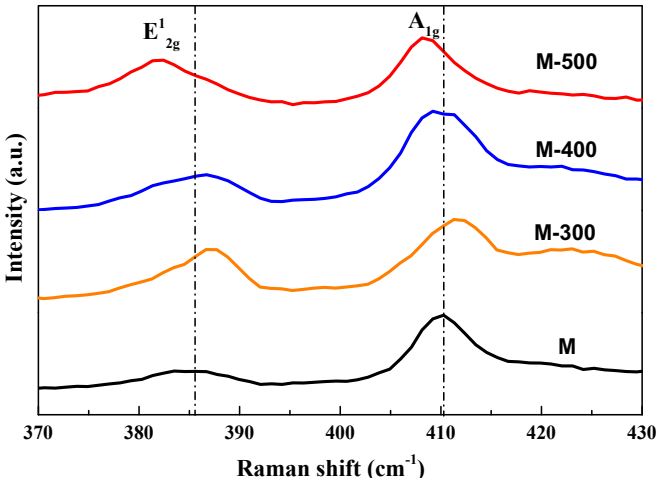

Fig. 2. Raman spectrum of molybdenite before and after thermal treatment.

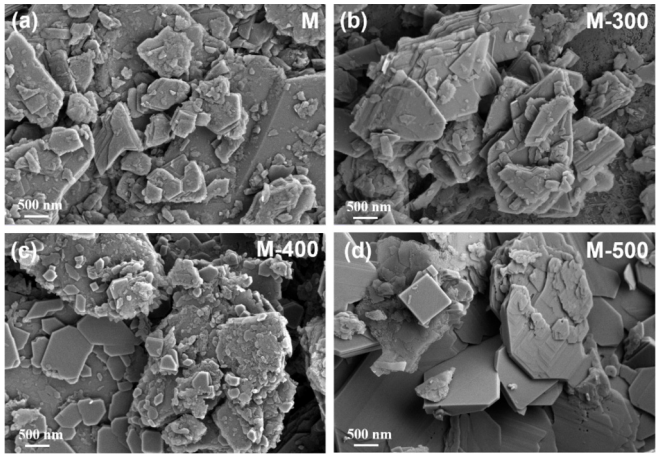

Fig. 3. SEM images of molybdenite (a) without thermal treatment, (b) thermally treated at 300 °C, (c) thermally treated at 400 °C and (d) thermally treated at 500 °C.

morphologies of samples, as shown in Fig. 5. Fig. 5a demonstrated that molybdenite before thermal modification was quite smooth. After thermal treatment of 300 °C (Fig. 5b), the inserted figure revealed the thickness of underlined area, indicating the uneven of surface of MoS_2 under the nanoscale observation. After thermal modification at 400 °C (Fig. 5c), lots of small triangular morphologies appeared on the surface of molybdenum. Meanwhile, the thickness in the corresponding insert figure was around 0.6 nm, which was in consistent with of thickness of monolayer molybdenite, demonstrating the formation of large quantities of triangular vacancies which contained a wealth of unsaturated S atoms on the edges. As a comparison, M-500 (Fig. 5d) was burned out with several layers which possessed less amount of sulfur vacancies than M-400. Interestingly, it was clear that in M-500, the triangular vacancies emerged in each two adjacent layers showed opposite orientations, which might be contributed to the dislocation of two adjacent layers of atoms in 2H-MoS_2 structure. In conclusion, sulfur vacancies teemed on the surface of molybdenite under 400 °C thermal modification.

In Fig. 6, XPS spectra for molybdenite with and without thermal modification was analyzed for determining the chemical composition. Fig. 6a displayed the Mo_{3d} spectra of molybdenite before and after thermal treatment. There exited two characteristic peaks of

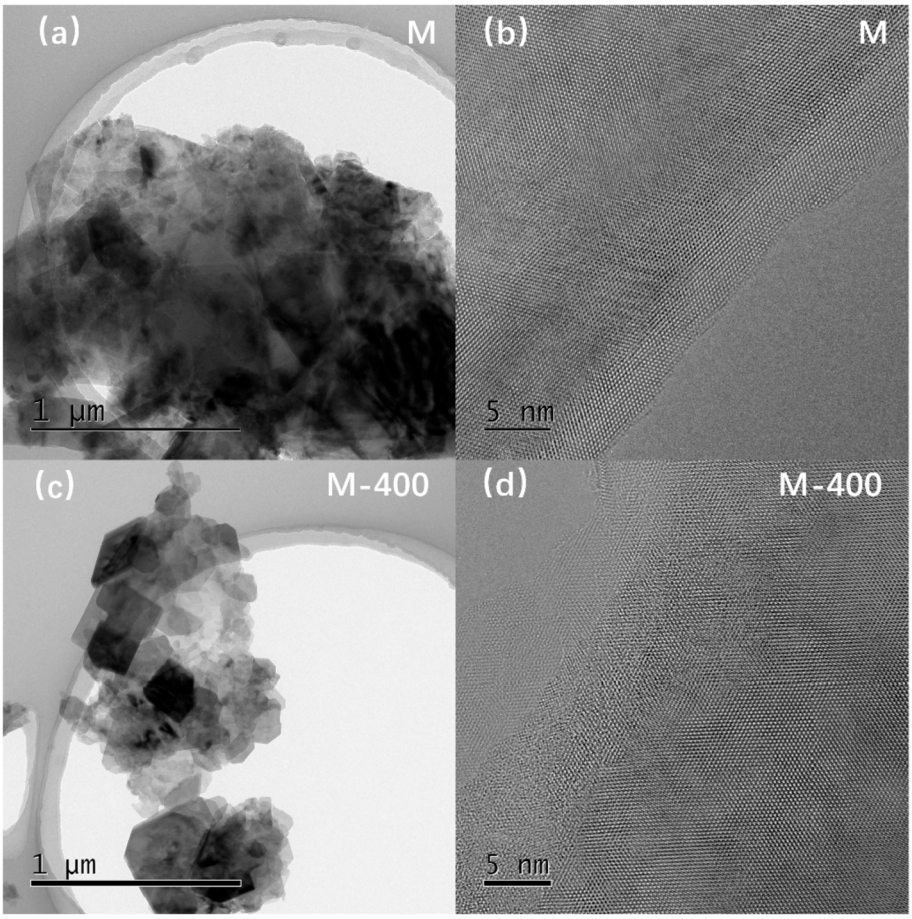

Fig. 4. TEM and HRTEM images of molybdenite without thermal treatment (a–b) and thermally treated at 400 °C (c–d).

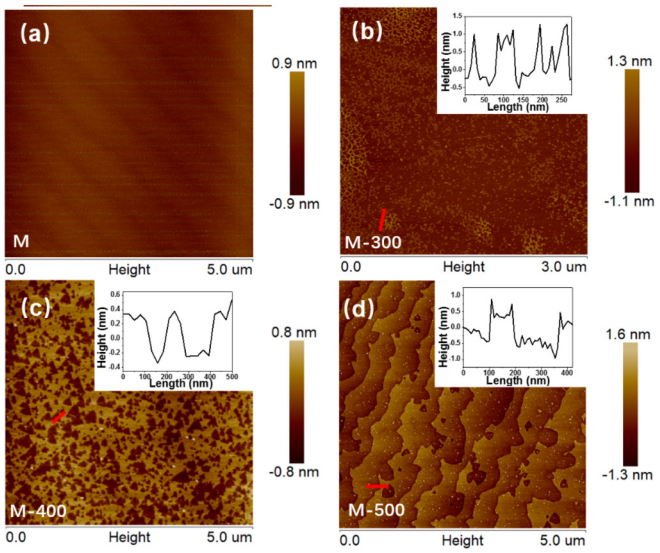

Fig. 5. AFM characterization of molybdenite without thermal treatment (a) and thermally treated at 300 °C (b), 400 °C (c) and 500 °C (d), respectively.

MoS_2 at around 232 eV, 229 eV and a S_{2s} peak at 226 eV on M(Wang et al., 1997; Yuan et al., 2019). After being thermally treated at 400 °C and 500 °C, a new peak cleared appeared at around 236 eV which was corresponded to MoO_3, indicating the partial transformation of MoS_2 to MoO_3(Jia et al., 2018a). The peak of MoO_3 became more remarkable with the augment of heating temperature. No peaks of MoO_3 was detected might due to the small content of MoO_3. The S_{2s} spectrum of molybdenite before and after thermal modification were shown in Fig. 6b. Peaks at about 162 and 163 eV were corresponded to S_{2s} in MoS_2, while the newly appeared peak at 165 eV at 400 °C thermal treatment was assigned to S_{2s} in MoS_3(Liu et al., 2017). The peaks of MoS_2 in M-300 and M-500 shifted owing to the interaction between MoO_3 and MoS_2 on the surface, however not obvious in M-400 might due to large exposure of monolayer MoS_2 on the surface. The valence states of Mo in MoS_2 and MoS_3 were the same, indicating the partially oxidized after thermal modification. From the O_{1s} spectrum (Fig. 6c), The peak around 530 eV originated from the H_2O. A new peak at around 530 eV could ascribe to the MoO_3 in molybdenite after thermal modification (Zhang et al., 2017). In conclusion, after thermal treatment of molybdenite, MoO_3 would generated and increased as the treatment temperature dilated.

Thermogravimetry analysis (TGA) of molybdenite in air atmosphere was displayed in Fig. 7. After being heated to 200 °C, molybdenite began to lose weight, suggesting that MoS_2 transformed to MoO_3. When molybdenite was heated to 450 °C, the weight lost quickly, which demonstrated that more MoO_3 generated. Around 9.78% weight was lost when molybdenite was heated to 600 °C, which was equal to the weight loss if all MoS_2 transformed into MoO_3.

As is wildly known that the hydrophobic property of absorbent was a fatal factor in absorption experiments, the contact angle tests

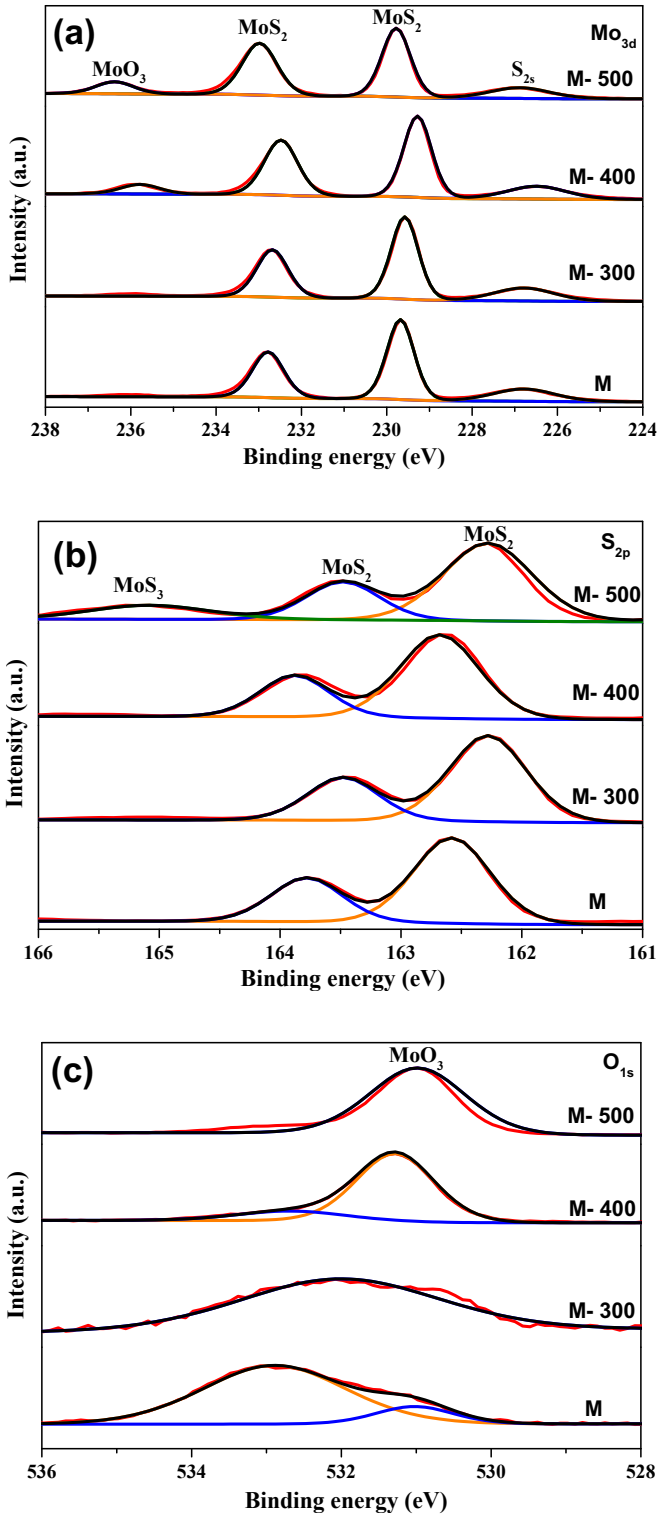

Fig. 6. XPS spectra of molybdenite with and without thermal modification: (a) Mo_{3d} XPS spectrum, (b) S_{2p} XPS spectrum, (c) O_{1s} XPS spectrum.

were carried out to investigate whether the hydrophobic property of molybdenite would differ between samples due to the hydrophilic property of the exposed Mo atoms generated on molybdenite during the thermal treatments. As shown in Fig. 8, the contact angle of natural molybdenite was 58°, while decreased to smaller angles (43°, 29° and 14°, respectively) as the thermal treatment

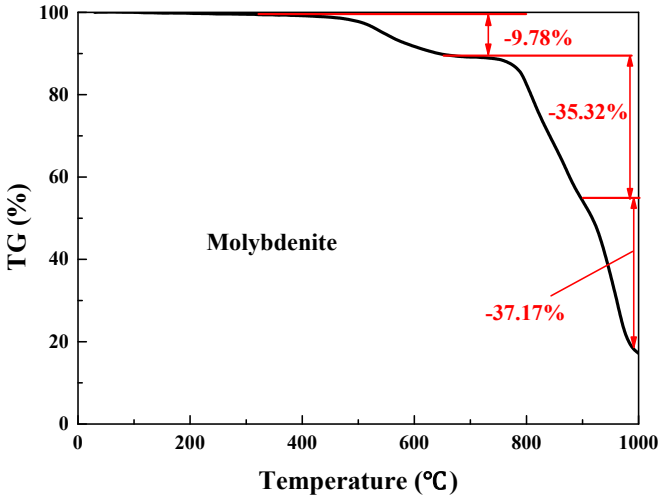

Fig. 7. Thermogravimetry analysis (TGA) of molybdenite in air atmosphere.

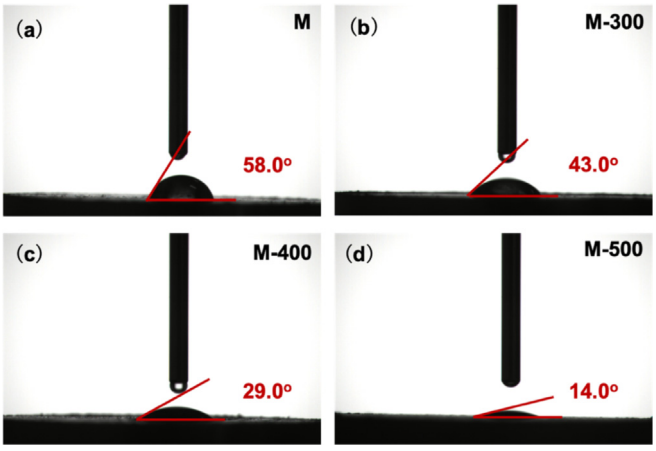

Fig. 8. Contact angle of molybdenum molybdenite without thermal treatment (a) and thermally treated at 300 °C (b), 400 °C (c) and 500 °C (d), respectively.

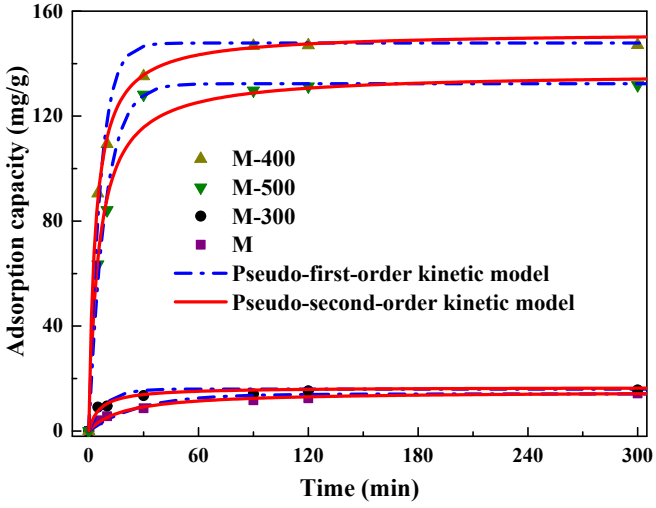

Fig. 9. Adsorption kinetics of Pb(II) on molybdenite before and after thermal treatment.

Table 1
Parameters of kinetics models of Pb(II) adsorption on molybdenite before and after thermal modification.

Adsorbent	Pseudo-first-kinetic model			Pseudo-second-kinetic model		
	k_1 (min^{-1})	q_{e1} (mg/g)	R_1^2	k_2 (g/(mg·min))	q_{e2} (mg/g)	R_2^2
M	0.037	14.114	0.946	0.003	15.150	0.989
M-300	0.113	15.992	0.913	0.010	16.657	0.960
M-400	0.160	147.846	0.982	0.002	151.945	0.999
M-500	0.113	132.346	0.994	0.001	136.522	0.988

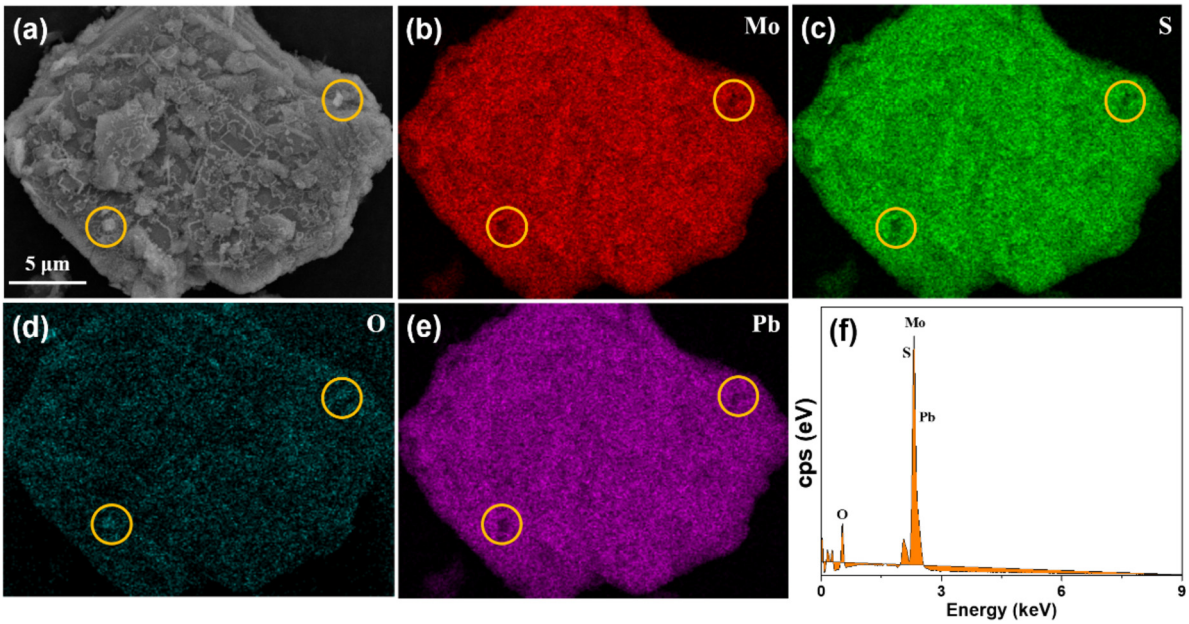

Fig. 10. SEM-EDS results of Pb(II) loaded M-400. (a) SEM image of Pb(II) loaded M-400, (b–e) EDS elemental mapping images of Mo, S, O and Pb, respectively, (e) EDX spectrum obtained from SEM image.

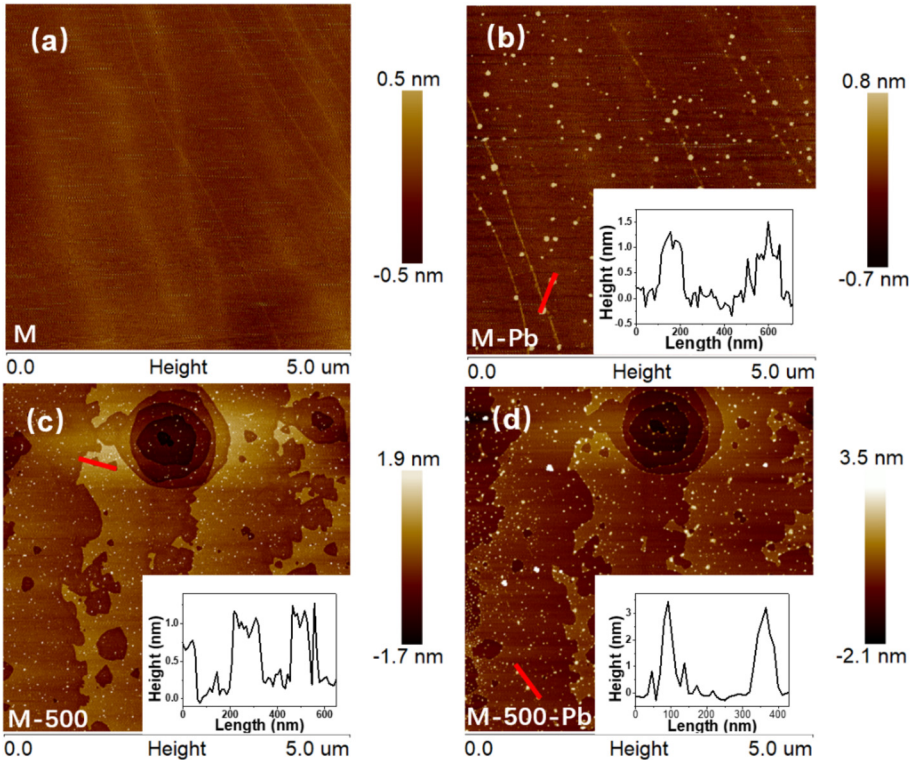

Fig. 11. AFM images of Pb(II) adsorption for 1 min on molybdenite without (a–b) and with thermal modification (c–d) before and after adsorption.

temperature increased, which might due to that more exposed Mo would generate under higher temperature.

3.2. Adsorption of Pb(II) on molybdenite before and after thermal treatment modification

Adsorption kinetics of Pb(II) on molybdenite before and after thermal treatment were carried out in Pb(II) solution with concentration of 100 mg/L and pH of 5.0. The adsorption capacity of Pb(II) on adsorbents as a function of adsorption time was exhibited in Fig. 9. It was obvious that the adsorption occurred very fast in the first 30 min, achieving an equilibrium within only 50 min. This might attribute to the exposure of the abundant sulfur sites on molybdenite. It was clear that M exhibited the lowest adsorption capacity at 15.31 mg/L, and M-300 (18.081 mg/L) had only a slight improvement than M. While the M-400 showed the largest adsorption at 152.67 mg/L, which was almost 10 times to M. The above results indicated that hydrophilic properties had little effect on the adsorption of Pb(II), and sulfur vacancy on the edges of molybdenite could significantly improve the Pb(II) adsorption capacity. Pseudo-first-order kinetic model and pseudo-second-order (Table 1) were applied for simulating the experimental data to study the mechanism of adsorption, and the results were given in Table 1. Pseudo-second-order kinetic model could well describe Pb(II) adsorption on all the samples because of the high correlation coefficient of R_2^2, demonstrating that chemical sorption or chemisorption including valence forces by sharing or exchanging of electrons might exist in between adsorbent and adsorbate.

SEM-EDS was applied for investigating Pb(II) adsorption on molybdenite after thermal treatment. Fig. 10 showed the EDS elemental of Mo, S, O and Pb on the surface of M-400 after Pb(II) adsorption at an initial concentration of 100 mg/L for 24 h. Fig. 10e generated by EDX analysis of Fig. 10a consist of spectra with peaks according to all the different elements. It demonstrated that the Pb(II) adsorption on molybdenite after thermal modification was made-up of Mo, S, O and Pb. In addition, it was clear that relatively white particles were generated after thermal treatment at 400 °C as circled in Fig. 10, which could ascribe to MoO_3 according to the uniform element distribution of Mo and O. A part of MoO_3 evaporated, and another left on the surface of MoS_2. After adsorption of Pb(II), element of Pb distribute little on MoO_3 areas but many on the surface of molybdenite, indicating that the increased Pb(II) adsorption on molybdenite was not owing to MoO_3.

3.3. Adsorption mechanism of Pb(II) on molybdenite after thermal modification

To further investigate what promoted the adsorption on molybdenite after thermal treatment, AFM and XPS were applied to study the adsorption of Pb(II) on molybdenite after thermal modification. AFM (Fig. 11) was used for better understanding on the Pb(II) adsorption on molybdenite after thermal modification. It's worth noting that M-500 with clear and long linear vacancies was chosen to observe the Pb(II) adsorption cites. Molybdenite possessed a smooth surface before thermal treatment (Fig. 11a), after being exposed to Pb(II) solution for 1 min, small substances were captured on the surface (Fig. 11b). The results indicated that the surface of molybdenite had an adsorption of Pb(II). As for M-500 (Fig. 11c), it could be seen that defects existed on molybdenite after thermal modification. After Pb(II) adsorption for 1 min, plenty of Pb(II) particles distributed on the surface of M-500 (Fig. 11d). In addition, the corresponding insert thickness picture also demonstrated the results that M-500 could well adsorb Pb(II). It was clear in Fig. 11d that Pb(II) teemed on edges of molybdenite, *i.e.*, Pb(II) ions were prone to react with the sulfur vacancies on edges of molybdenite, demonstrating that sulfur vacancy could bring a significant enhancement on the Pb(II) adsorption.

XPS was carried out to study the adsorption mechanism of Pb(II) on molybdenite with and without thermal treatment, as exhibited in Fig. 12. The Pb_{4f} (Fig. 12a) XPS spectrum appeared at around 140 eV and 139 eV could be assigned to Pb-S (Kovalev et al., 2010),

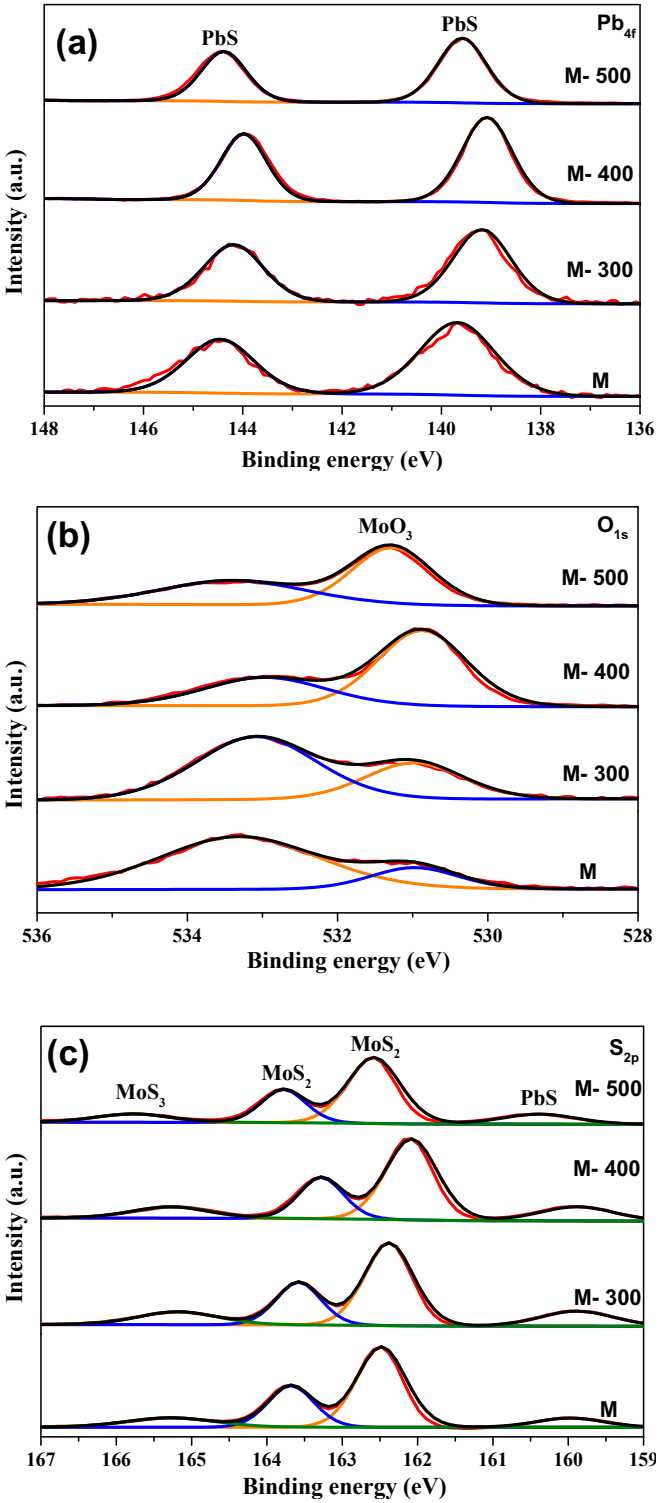

Fig. 12. XPS spectra of molybdenite with and without thermal modification after adsorption of Pb(II): (a) Pb_{4f} XPS spectrum, (b) O_{1s} XPS spectrum, (c) S_{2p} XPS spectrum.

which gave a clear evidence for the Pb adsorption on molybdenite with and without thermal modification. No peak at about 173 eV appeared (Liu et al., 2017), demonstrating the MoO_3 had a weak affinity with Pb. Meanwhile, from O_{1s} spectrum (Fig. 12b), no new peaks appeared, showing that no Pb-O bond generated. Fig. 12c showed the S_{2p} spectrum, which could be divided into four peaks. The peak at 160 eV was derived from PbS, and the peaks at 162 eV and 163 eV was originated from MoS_2, another peak at 165 eV was MoS_3. Thus, in the process of Pb(II) adsorption on molybdenite with and without thermal modification, the main interaction between Pb and adsorbent was between Pb and S atoms, S vacancy would strengthen the interaction which achieved better adsorption. Thus, the experiment indicated that the increase of surface hydrophilia of molybdenite would benefit the Pb(II) adsorption. Meanwhile, sulfur atoms exposed at the triangular edges of molybdenite were the intrinsic reason for the great enhancement of Pb(II) adsorption.

4. Conclusions

In this work, a facile thermal treatment method was proposed for producing large quantities of S vacancies on the edges of molybdenite to greatly enhance the adsorption of Pb(II). The results illustrated that the molybdenite after thermal modification could achieve a Pb(II) adsorption capacity of 147.846 mg/g, which was almost 10 times to that of pristine. The hydrophobic property had little effect on the adsorption of Pb(II) but S vacancy on edges of molybdenite could facilitate the adsorption. The adsorption mechanism was that S atoms especially S vacancies on edges had strong affinity to Pb ions, thus achieving a great enhancement of Pb(II) adsorption to Molybdenite.

Declaration of competing interest

There are no conflicts of interest to declare.

CRediT authorship contribution statement

Yuan Yuan: Conceptualization, Methodology, Writing - original draft. **Weiquan Zhan:** Supervision, Investigation. **Feifei Jia:** Formal analysis, Validation. **Shaoxian Song:** Data curation.

Acknowledgements

The financial supports to this work from the National Natural Science Foundation of China (Nos. 51974216, 51704212 and 51704220), the Natural Science Foundation of Hubei Province (No. 2019CFB536), and the Research Fund Program of Key Laboratory of Rare Mineral, Ministry of Land and Resources (KLRM-KF201802) are gratefully acknowledged.

References

Abbaspour, A., Mirahmadi, E., Khalafi-nejad, A., Babamohammadi, S., 2010. A highly selective and sensitive disposable carbon composite PVC-based membrane for determination of lead ion in environmental samples. J. Hazard Mater. 174, 656–661. https://doi.org/10.1016/j.jhazmat.2009.09.101.

Ai, K., Ruan, C., Shen, M., Lu, L., 2016. MoS2 nanosheets with widened interlayer spacing for high-efficiency removal of mercury in aquatic systems. Adv. Funct. Mater. 26, 5542–5549. https://doi.org/10.1002/adfm.201601338.

Alvarez, M.T., Crespo, C., Mattiasson, B., 2007. Precipitation of Zn(II), Cu(II) and Pb(II) at bench-scale using biogenic hydrogen sulfide from the utilization of volatile fatty acids. Chemosphere 66, 1677–1683. https://doi.org/10.1016/j.chemosphere.2006.07.065.

Ding, R., Krikstolaityte, V., Lisak, G., 2019. Inorganic salt modified paper substrates utilized in paper based microfluidic sampling for potentiometric determination of heavy metals. Sensor. Actuator. B Chem. 290, 347–356. https://doi.org/10.1016/j.snb.2019.03.079.

Feng, Q., Wen, S., Deng, J., Zhao, W., 2017. Combined DFT and XPS investigation of enhanced adsorption of sulfide species onto cerussite by surface modification with chloride. Appl. Surf. Sci. 425, 8–15. https://doi.org/10.1016/j.apsusc.2017.07.017.

Gao, M.R., Chan, M.K.Y., Sun, Y., 2015. Edge-terminated molybdenum disulfide with a 9.4-Å interlayer spacing for electrochemical hydrogen production. Nat. Commun. 6, 1–8. https://doi.org/10.1038/ncomms8493.

Gatabi, J., Sarra, Y., Mansour, M., Taghavi, M., 2020. Chemosphere Facile and Ef Fi Cient Removal of Pb (II) from Aqueous Solution by Chitosan-Lead Ion Imprinted Polymer Network 240. https://doi.org/10.1016/j.chemosphere.2019.124772.

Hong, M., Shi, J., Huan, Y., Xie, Q., Zhang, Y., 2019. Microscopic insights into the catalytic mechanisms of monolayer MoS2 and its heterostructures in hydrogen evolution reaction. Nano Res 12, 2140–2149. https://doi.org/10.1007/s12274-019-2370-3.

Hong, X., Kim, J., Shi, S.F., Zhang, Yu, Jin, C., Sun, Y., Tongay, S., Wu, J., Zhang, Yanfeng, Wang, F., 2014. Ultrafast charge transfer in atomically thin MoS2/WS2 heterostructures. Nat. Nanotechnol. 9, 682–686. https://doi.org/10.1038/nnano.2014.167.

Hu, L., Yang, Z., Cui, L., Li, Y., Ngo, H.H., Wang, Y., Wei, Q., Ma, H., Yan, L., Du, B., 2016. Fabrication of hyperbranched polyamine functionalized graphene for high-efficiency removal of Pb(II) and methylene blue. Chem. Eng. J. 287, 545–556. https://doi.org/10.1016/j.cej.2015.11.059.

Huang, N., Zhai, L., Xu, H., Jiang, D., 2017. Stable covalent organic frameworks for exceptional mercury removal from aqueous solutions. J. Am. Chem. Soc. 139, 2428–2434. https://doi.org/10.1021/jacs.6b12328.

Huang, X., Zhao, H., Zhang, G., Li, J., Yang, Y., Ji, P., 2020. Potential of removing Cd(II) and Pb(II) from contaminated water using a newly modified fly ash. Chemosphere 242, 125148. https://doi.org/10.1016/j.chemosphere.2019.125148.

Jeffrey, M.I., Hewitt, D.M., Dai, X., Brunt, S.D., 2010. Ion exchange adsorption and elution for recovering gold thiosulfate from leach solutions. Hydrometallurgy 100, 136–143. https://doi.org/10.1016/j.hydromet.2009.11.003.

Jia, F., Liu, C., Yang, B., Zhang, X., Yi, H., Ni, J., Song, S., 2018a. Thermal modification of molybdenum disulfide surface for tremendous improvement of Hg2+ adsorption from aqueous solution. ACS Sustain. Chem. Eng. 6, 9065–9073. https://doi.org/10.1021/acssuschemeng.8b01412.

Jia, F., Sun, K., Yang, B., Zhang, X., Wang, Q., Song, S., 2018b. Defect-rich molybdenum disulfide as electrode for enhanced capacitive deionization from water. Desalination 446, 21–30. https://doi.org/10.1016/j.desal.2018.08.024.

Jia, F., Wang, Q., Wu, J., Li, Y., Song, S., 2017. Two-Dimensional molybdenum disulfide as a superb adsorbent for removing Hg2+ from water. ACS Sustain. Chem. Eng. 5, 7410–7419. https://doi.org/10.1021/acssuschemeng.7b01880.

Kovalev, A.I., Wainstein, D.L., Rashkovskiy, A.Y., Osherov, A., Golan, Y., 2010. Size shift of XPS lines observed from PbS nanocrystals. Surf. Interface Anal. 42, 850–854. https://doi.org/10.1002/sia.3243.

Kumar, N., Fosso-Kankeu, E., Ray, S.S., 2019. Achieving controllable MoS2 nanostructures with increased interlayer spacing for efficient removal of Pb(II) from aquatic systems. ACS Appl. Mater. Interfaces 11, 19141–19155. https://doi.org/10.1021/acsami.9b03853.

Lisak, G., Bobacka, J., Lewenstam, A., 2012. Recovery of nanomolar detection limit of solid-contact lead (II)-selective electrodes by electrode conditioning. J. Solid State Electrochem. 16, 2983–2991. https://doi.org/10.1007/s10008-012-1725-4.

Liu, C., Jia, F., Wang, Q., Yang, B., Song, S., 2017. Two-dimensional Molybdenum Disulfide as Adsorbent for High-Efficient Pb(II) Removal from Water.

Liu, C., Wang, Q., Jia, F., Song, S., 2019. Adsorption of heavy metals on molybdenum disulfide in water: a critical review. J. Mol. Liq. 292, 111390. https://doi.org/10.1016/j.molliq.2019.111390.

Manohar, D.M., Krishnan, K.A., Anirudhan, T.S., 2002. Removal of mercury (II) from aqueous solutions and chlor-alkali industry wastewater using 2-mercaptobenzimidazole-clay. Water Res. 36, 1609–1619.

Mondal, B., Mahendranath, A., Som, A., Bose, S., Ahuja, T., Kumar, A.A., Ghosh, J., Pradeep, T., 2018. Rapid reaction of MoS2 nanosheets with Pb2+ and Pb4+ ions in solution. Nanoscale 10, 1807–1814. https://doi.org/10.1039/c7nr07523e.

Peng, W., Li, H., Liu, Y., Song, S., 2016. Comparison of Pb(II) adsorption onto graphene oxide prepared from natural graphites: diagramming the Pb(II) adsorption sites. Appl. Surf. Sci. 364, 620–627. https://doi.org/10.1016/j.apsusc.2015.12.208.

Saénz, M., Fernández, L., Domínguez, J., Alvarado, J., 2010. Electrochemical generation of lead volatile species as a method of sample introduction for lead determination by atomic absorption spectrometry. Electroanalysis 22, 2842–2847. https://doi.org/10.1002/elan.201000333.

Sdiri, A., Higashi, T., Chaabouni, R., Jamoussi, F., 2012. Competitive removal of heavy metals from aqueous solutions by montmorillonitic and calcareous clays. Water Air Soil Pollut. 223, 1191–1204. https://doi.org/10.1007/s11270-011-0937-z.

Sun, K., Jia, F., Yang, B., Lin, C., Li, X., Song, S., 2019. Synergistic effect in the reduction of Cr(VI) with Ag-MoS2 as photocatalyst. Appl. Mater. Today 2, 100453. https://doi.org/10.1016/j.apmt.2019.100453.

Tang, B., Yu, Z.G., Seng, H.L., Zhang, N., Liu, X., Zhang, Y., Yang, W., Gong, H., 2018. Simultaneous edge and electronic control of MoS2 nanosheets through Fe doping for an efficient oxygen evolution reaction. Nanoscale 10, 20113–20119. https://doi.org/10.1039/c8nr06659k.

Wang, H.W., Skeldon, P., Thompson, G.E., 1997. XPS studies of MoS2 formation from ammonium tetrathiomolybdate solutions. Surf. Coating. Technol. 91, 200–207. https://doi.org/10.1016/S0257-8972(96)03186-6.

Wang, J., Wang, P., Wang, H., Dong, J., Chen, W., Wang, Xiangxue, Wang, S., Hayat, T., Alsaedi, A., Wang, Xiangke, 2017. Preparation of molybdenum disulfide coated Mg/Al layered double hydroxide composites for efficient removal of

chromium(VI). ACS Sustain. Chem. Eng. 5, 7165–7174. https://doi.org/10.1021/acssuschemeng.7b01347.
Wang, Q., Yang, L., Jia, F., Li, Y., Song, S., 2018. Removal of Cd (II) from water by using nano-scale molybdenum disulphide sheets as adsorbents. J. Mol. Liq. 263, 526–533. https://doi.org/10.1016/j.molliq.2018.04.149.
Xu, Q., Wang, Yulu, Jin, L., Wang, Yu, Qin, M., 2017. Adsorption of Cu (II), Pb (II) and Cr (VI) from aqueous solutions using black wattle tannin-immobilized nano-cellulose. J. Hazard Mater. 339, 91–99. https://doi.org/10.1016/j.jhazmat.2017.06.005.
Yin, N., Wang, K., Wang, L., Li, Z., 2016. Amino-functionalized MOFs combining ceramic membrane ultrafiltration for Pb (II) removal. Chem. Eng. J. 306, 619–628. https://doi.org/10.1016/j.cej.2016.07.064.
Yuan, Y., Yang, B., Jia, F., Song, S., 2019. Reduction mechanism of Au metal ions into Au nanoparticles on molybdenum disulfide. Nanoscale 11, 9488–9497. https://doi.org/10.1039/c8nr09420a.
Zeng, H., Wang, L., Zhang, D., Yan, P., Nie, J., Sharma, V.K., Wang, C., 2019. Highly efficient and selective removal of mercury ions using hyperbranched polyethylenimine functionalized carboxymethyl chitosan composite adsorbent. Chem. Eng. J. 358, 253–263. https://doi.org/10.1016/j.cej.2018.10.001.
Zhan, W., Jia, F., Yuan, Y., Liu, C., Sun, K., Yang, B., 2020. Controllable incorporation of oxygen in MoS2 for efficient adsorption of Hg2+ in aqueous solutions. J. Hazard Mater. 384, 1–10. https://doi.org/10.1016/j.jhazmat.2019.121382.
Zhang, D., Wang, L., Zeng, H., Yan, P., Nie, J., Sharma, V.K., Wang, C., 2019. A three-dimensional macroporous network structured chitosan/cellulose biocomposite sponge for rapid and selective removal of mercury(II) ions from aqueous solution. Chem. Eng. J. 192–202. https://doi.org/10.1016/j.cej.2019.01.127.
Zhang, X., Jia, F., Yang, B., Song, S., 2017. Oxidation of molybdenum disulfide sheet in water under in situ atomic force microscopy observation. J. Phys. Chem. C 121, 9938–9943. https://doi.org/10.1021/acs.jpcc.7b01863.
Zhu, H., Tan, X., Tan, L., Zhang, H., Liu, H., Fang, M., Hayat, T., Wang, X., 2018. Magnetic porous polymers prepared via high internal phase emulsions for efficient removal of Pb2+ and Cd2+. ACS Sustain. Chem. Eng. 6, 5206–5213. https://doi.org/10.1021/acssuschemeng.7b04868.